CRYSTAL GROWTH & DESIGN
2003
VOL. 3, NO. 3
375−382

Role of Polymorphous Metastability in Crystal Formation Kinetics of 2,3,6,7,10,11-Hexa(4′-Octyloxybenzoyloxy)-Triphenylene Discotic Molecules

Benjamin Y. Tang,[†] Alexander J. Jing,[†] Christopher Y. Li,[‡] Zhihao Shen,[†] Huabin Wang,[†] Frank W. Harris,[†] and Stephen Z. D. Cheng*,[†]

Maurice Morton Institute and Department of Polymer Science, The University of Akron, Akron, Ohio 44325-3909, and Department of Materials Engineering, Drexel University, Philadelphia, Pennsylvania 19104

Received December 18, 2002

ABSTRACT: Phase transition behaviors of a discotic liquid crystal 2,3,6,7,10,11-hexa(4′-octyloxybenzoyloxy)-triphenylene (HOBT-C8) were investigated. Four phases having different orders and symmetries existed in this system: a discotic nematic phase, a rectangular columnar (ColR) phase, an orthorhombic crystalline (CrI) phase developed upon cooling, and a monoclinic crystalline (CrII) phase formed during heating (Tang, B. Y., et al. *Mater. Chem.* **2001**, *13*, 78). The CrI phase represented a metastable phase compared to the CrII phase. On the basis of the results of differential scanning calorimetry, wide-angle X-ray diffraction, and polarized light microscopy (PLM) experiments, three crystallization-temperature (T_c) regions were identified to help study the crystallization kinetics of the CrI and CrII phases. In the large T_c region below 114 °C (region III), the CrI phase formed first despite its metastable nature (monotropic) due to the faster crystallization kinetics of the ColR → CrI phase in this region. The CrI → CrII phase transformation then followed. However, when the $T_c \geq 115$ °C in region I, which was close to the melting temperature (T_m) of the CrI phase ($T_m = 121$ °C), only the CrII phase formed directly from the ColR phase. In the narrow T_c region II where 114 °C $\leq T_c <$ 115 °C, primary nucleation and overall crystallization rates of CrI and CrII phases were reversed. Linear crystal growth rate measurements in PLM revealed that a minimum in the CrII phase growth rate was found in region II. This indicated that as long as the growth rates of both phases were similar and on the same growth front, the CrII phase formation could be hampered by the growth of the metastable CrI phase.

Introduction

The discovery of discotic liquid crystals (LCs) and their columnar phases has led to a variety of new developments in molecular and supramolecular architectures.[2−16] Classification of these new discotic liquid crystalline phases has paralleled those of rodlike LCs, and they may exhibit low ordered nematic (ND) as well as various high ordered columnar (Col) phases.[2,4,5] In the ND phase, the disklike molecules only have orientational order with the molecular short axis aligning, on average, parallel to the director (perpendicular to the disk plane). In the ordered liquid crystalline Col phases, the lateral packing can range from rectangular (ColR), to hexagonal (ColH), tilted, or oblique phases.[3−5,17−21] Other nondisc-shaped molecules[12−14] and liquid crystalline polymers with rodlike mesogens[22−26] can also assemble into various Col phases.

When LCs display polymorphism, the exhibition of multiple liquid crystalline and crystalline phase transitions, monotropic phase behavior may sometimes be observed.[27−35] This behavior has also been reported in ColH phases of a series of metallomesogenic discotic LCs.[11] The monotropic phase exists only when the more stable phase is bypassed because the necessity of undercooling is required to overcome the free energy barrier in forming this stable phase during cooling.

Recent research has shown discotic LCs containing triphenylenes can be modified to have potential applications in developing compensation layers with a highly tilted optical axis (>30°) in LC displays.[36] We have reported complicated phase transition behaviors of a discotic LC compound, 2,3,6,7,10,11-hexa(4′-octyloxybenzoyloxy)-triphenylene, abbreviated as HOBT-C8.[1] It was observed that this discotic LC exhibited complicated polymorphism: a ND phase existed at temperatures above 171 °C, a rectangular columnar (ColR) phase between 151 and 171 °C, an orthorhombic crystalline (CrI) phase with a melting temperature (T_m) of 121 °C developed upon cooling, and a monoclinic crystalline (CrII) phase with a T_m of 151 °C formed during heating.[1] Therefore, the CrI phase represented a metastable phase compared to the CrII phase. The transition sequence during cooling and heating are

$$\mathrm{I} \xrightarrow[0.5\ \mathrm{J/mol}]{239\ ^\circ\mathrm{C}} \mathrm{ND} \xrightarrow[6.1\ \mathrm{kJ/mol}]{171\ ^\circ\mathrm{C}} \mathrm{ColR} \xrightarrow[5.6\ \mathrm{kJ/mol}]{102\text{ - }112\ ^\circ\mathrm{C}} \mathrm{CrI} \xrightarrow{\text{Very slow cooling}} \mathrm{CrII}$$

$$\mathrm{CrI} \xrightarrow{121\ ^\circ\mathrm{C}} \mathrm{CrII} \xrightarrow[19.9\ \mathrm{kJ/mol}]{151\ ^\circ\mathrm{C}} \mathrm{ColR} \xrightarrow[6.1\ \mathrm{kJ/mol}]{171\ ^\circ\mathrm{C}} \mathrm{ND} \xrightarrow[0.5\ \mathrm{J/mol}]{239\ ^\circ\mathrm{C}} \mathrm{I}$$

In this paper, we attempt to address the kinetic issue of these phase transformations. Specifically, we will focus on the aspects involving the monotropic metastable CrI phase formation and its role and effect on the CrII phase formation.

* To whom correspondence should be addressed. E-mail: scheng@uakron.edu.
[†] The University of Akron.
[‡] Drexel University.

10.1021/cg020069d CCC: $25.00
Published on Web 03/20/2003

Experimental Section

Material and Sample Preparations. The discotic LC compound HOBT-C8 was synthesized and purified following the procedure described in ref 5. The chemical structure is

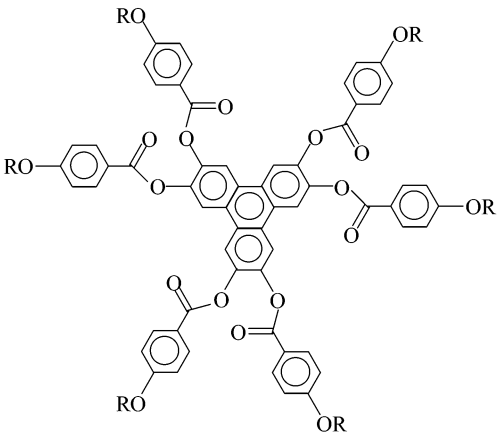

R = -$(CH_2)_7$-CH_3

The molecular mass was 1932 g/mol. The sample was vacuum-dried before carrying out any characterization or analysis. For differential scanning calorimetry (DSC) experiments at heating and cooling rates of equal or slower than 10 °C/min, the sample weight was about 2.5 mg and the pan weights were kept constant with a precision of ± 0.001 mg. Upon increasing in the scanning rates, the sample weights were correspondingly decreased to avoid instrumental lag. To determine the different phase transformation kinetics, samples having a thickness of around 0.5 mm for time-resolved wide-angle X-ray diffraction (WAXD) powder (one-dimensional, 1D) experiments were prepared. For the polarized light microscopy (PLM) experiments, the molten samples were sandwiched between a glass and cover slide, and the sample thickness was controlled to be 10 μm.

The isotropization of HOBT-C8 occurred at a high temperature of 239 °C with a heat of transition of the ND → I of 0.5 kJ/mol measured by DSC. To avoid sample decomposition and oxidation while still eliminating the previous thermal history, the samples for DSC and WAXD experiments performed in this study were only heated to 180 °C in the ND phase instead of the I. The sample fluidity was high and the sample was almost transparent in the ND phase.

Equipment and Experiments. A Perkin-Elmer DSC-7 with a cooling refrigerator was used for DSC experiments. The calibration of temperature and heat of transition was performed using standard materials (benzoic acid and indium) at different scanning rates. To investigate isothermal crystallization kinetics, the samples were quenched from the ND phase to the preset isothermal crystallization temperature (T_c) so that the exothermic process could be recorded with respect to crystallization time (t_c). For this sample, the ND → ColR transition was independent of the cooling rate and always formed at 171 °C.[1] The quenching rate was estimated to be ~100 °C/min. However, when the T_c was rather high (>112 °C), the exothermic process could not be directly observed using this method due to the prolonged transformation process. Therefore, a second method was used to observe the phase transition kinetics: the samples were again quenched from the ND phase to the preset isothermal T_c (> 112 °C) and after a prefixed t_c, the samples were directly heated to 180 °C without prior cooling. The heating rates were ranged from 1 to 80 °C/min to minimize the annealing effect. In this case, the endothermic processes recorded during heating represented the portions of the crystals that formed during this period of t_c at the T_c.

The WAXD experiments were carried out using a Rigaku 12 kW rotating anode (Cu K_α the wavelength is 0.154 nm) X-ray generator coupled with a goniometer and a hot stage. A graphite crystal was inserted into the beam as a monochromator and the beam was line-focused. The distance between the sample and the goniometer was set at 200 mm. The diffraction angle was calibrated using silicon powder crystals for the high angle region (2θ > 15°) and silver behenate crystals for the low angle region (2θ < 15°). The scanning rate was 7°/min and the structural developments during isothermal crystallization at different T_c values were recorded.

An Olympus (HB-2) PLM coupled with a Mettler (FP90) hot stage was utilized for optical texture observations. Isothermal crystallization experiments were carried out by inserting the sample that was preheated in another hot stage to the Mettler (FP90) at preset T_c values. The length scale of the PLM was calibrated using a length standard. Therefore, the crystal growth rates could be calculated by the ratio of the crystal growth distance to the time period spent to develop the crystals at different T_c values.

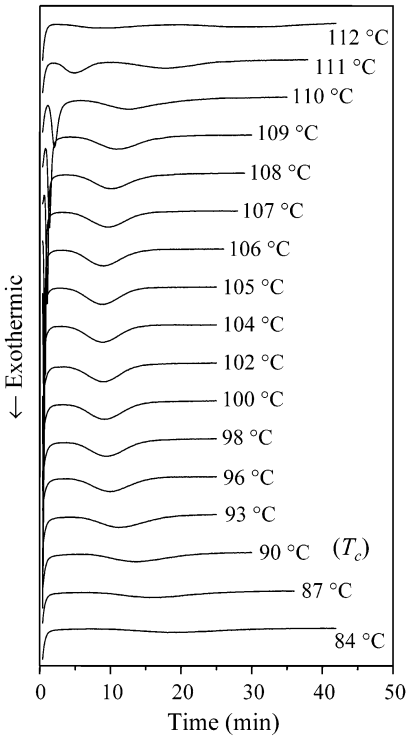

Figure 1. Set of isothermal DSC diagrams of HOBT-C8 at different T_c values ranging from 84 and 112 °C.

Results and Discussion

The ColR → CrI, the CrI → CrII, and the ColR → CrII Phase Evolutions. Figure 1 shows a set of isothermal DSC diagrams of HOBT-C8 at different T_c values. Below T_c = 104 °C, only one exothermic process was observed, which possessed a peak time of greater than 5 min. However, at T_c ≥ 104 °C, another fast exothermic process started to appear at a rather short time period. Therefore, above 104 °C two exothermic processes existed. A further increase of T_c to above 112 °C resulted in the exothermic processes not being clearly recognized in Figure 1 due to the very slow crystallization processes. Therefore, we needed to use the second method described in Experimental Section to characterize the phase transformation kinetics. To ensure that these two methods provide identical phase transformation kinetics, we have purposely carried out a study of using both methods at the same T_c.

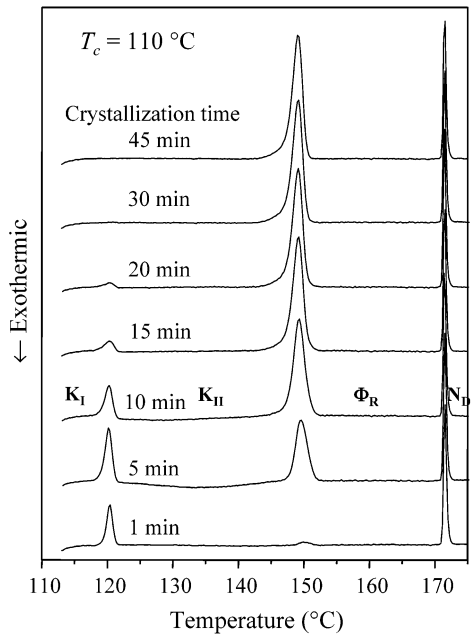

Figure 2. Set of DSC heating diagrams at 5 °C/min for HOBT-C8 after isothermally crystallized at T_c = 110 °C at different t_c values.

Figure 2 is the DSC heating diagrams after the HOBT-C8 sample was isothermally crystallized at T_c = 110 °C at different periods of time using the second method. The heating rate used in this figure was 5 °C/min, as an example. It is evident that the times of forming these two phases detected by the two methods are very close to each other in comparison to Figure 1. The DSC heating diagrams in Figure 2 also indicate the identical transition sequence, namely, the first phase formed through the ColR → CrI phase transformation as soon as the T_c was reached or even during the quenching. Note that the CrI phase crystal melted at a T_m of 121 °C. The latter formed phase after 1-min isothermal crystallization was the CrII phase, and it exhibited a T_m at 151 °C. The CrII phase formed before the maximum transition enthalpy of the CrI phase (5.6 kJ/mol, see below) was reached. This suggests that some degree of overlapping in the phase transformations may exist. It should also be noted that during heating in DSC experiments, the CrI phase could also be annealed into the CrII phase. This effect could be minimized when the heating rate of 80 °C/min was used.

Figure 3 shows a set of DSC heating diagrams at T_c = 113 °C. The CrI phase formed first when $t_c \leq 20$ min, and the CrII phase started to develop beyond t_c = 30 min. Although the CrI phase was observed until t_c = 100 min, the phase gradually diminished while the CrII phase continued to grow. This observation reveals that at 113 °C, although the primary nucleation rate of the ColR → CrI phase was faster than that of the ColR → CrII phase transformation, the transformation of the CrI → CrII phase occurred as soon as the CrI phase was established.

Figure 4 shows a set of DSC heating diagrams at different t_c values when the HOBT-C8 sample was isothermally crystallized at 114.5 °C. The first appearance at t_c = 50 min was the CrII phase at T_c = 114.5 °C which is different from Figures 2 and 3. The CrI phase appeared at t_c = 60 min. Since these DSC diagrams

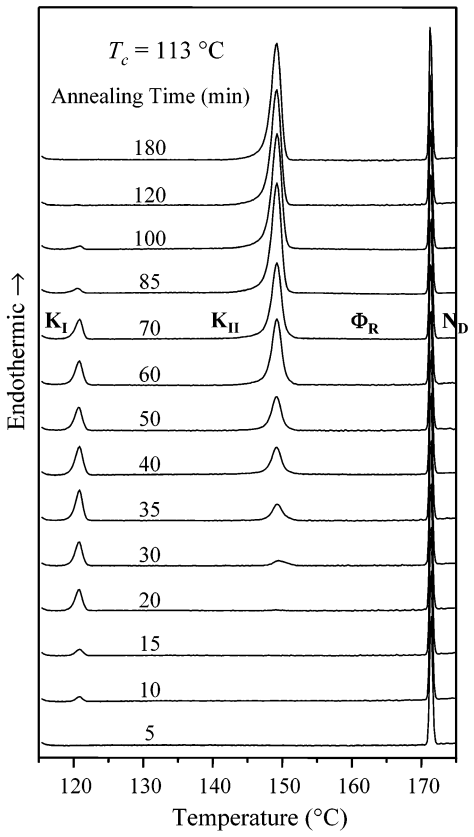

Figure 3. Set of DSC heating diagrams at 5 °C/min for HOBT-C8 after isothermally crystallized at T_c = 113 °C at different t_c values.

were recorded during heating at 5 °C/min, it could also be possible that the observed CrII phase at $t_c \leq 60$ min was due to an annealing transfer of the CrI phase to the CrII phase during heating. However, fast heating at 80 °C/min did not show the existence of the CrI phase after the sample was crystallized at t_c = 50 min. This suggests that the CrII phase observed in Figure 4 at t_c = 50 min grew directly from the ColR phase. The WAXD results also support this conclusion (see below). Therefore, we concluded that at T_c = 114.5 °C, the primary nucleation rate of the ColR → CrII phases was somewhat faster than that of the ColR → CrI phase transition. Namely, the primary nucleation barrier of the CrII phase formation was slightly lower than that of the CrI phase formation from the ColR phase. From a kinetic point of view, primary nuclei of the CrI phase can still form but in a slightly longer period of t_c. Nevertheless, the disappearance of the CrI phase after t_c = 115 min before the full development of this phase indicated that the transformation of the CrI → CrII phase did exist.

Figure 5 shows a set of DSC heating diagrams of a sample crystallized at T_c = 115 °C. It is evident that at this T_c the CrII phase grew directly from the ColR phase, which possesses a T_m of 151 °C. The CrI phase, which has a T_m of 121 °C, was not found.

Phase Identifications during the Transitions. Detailed phase structural determinations were carried out via extensive 2D WAXD and electron diffraction experiments as described in ref 1, and they provided characteristic diffractions of each phase in the low 2θ-angle region. Figure 6 shows a set of isothermal WAXD

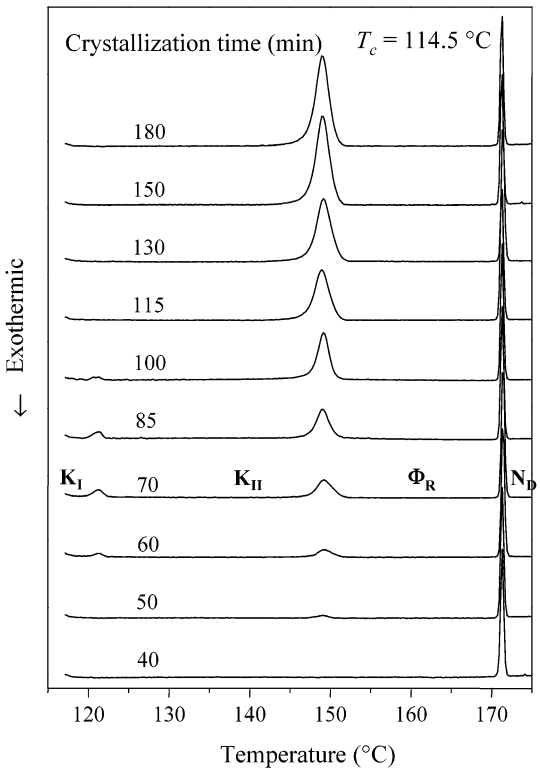

Figure 4. Set of DSC heating diagrams at 5 °C/min for HOBT-C8 after isothermally crystallized at T_c = 114.5 °C at different t_c values.

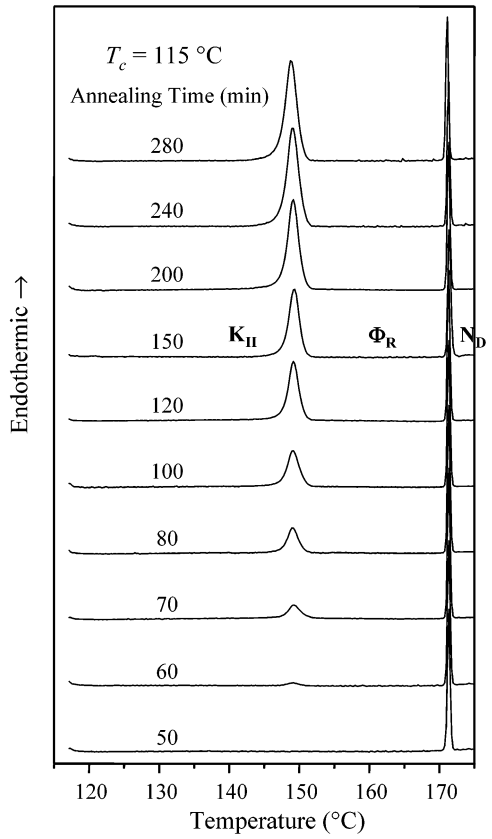

Figure 5. Set of DSC heating diagrams at 5 °C/min for HOBT-C8 after isothermally crystallized at T_c = 115 °C at different t_c values.

powder patterns of HOBT-C8 at T_c = 113 °C for different t_c values. We will only concentrate our attention on the results obtained in the low 2θ-angle region in this study since different phase structures exhibit their own characteristic diffractions. It should be noted that when these phase transitions take place, the domain size changes which, in turn, directly affects the widths of half-height of the diffraction peaks in the WAXD powder pattern of the ColR and crystalline phases. Furthermore, structural factors in different crystalline phases also vary. Therefore, we will only compare the intensity changes within each phase rather than between the phases.

In Figure 6, two overlapped reflections at 2θ = 3.6° and 3.7° in the low-2θ angle region were observed when the isothermal experiment was up to 5 min. These two peaks correspond to the (110) and (200) diffractions of the ColR phase based on the phase structural determination.[1] At t_c = 20 min, a reflection at 2θ = 3.2°, which was attributed to the (111) diffraction of the CrI phase appeared. However, the intensity of the (110) and (200) diffractions resulted from the ColR phase decreased due to the progressive formation of the CrI phase. The CrI phase lasted up to 100 min. When the t_c reached about 35 min (Figure 6), a small reflection at 2θ = 3.3° that was the strongest characteristic (200) diffraction of the CrII phase, started to appear.[1] The intensity of this diffraction (at 2θ = 3.3°) continuously increased and became a dominant reflection when t_c reached 140 min (Figure 6). Overlapping reflections having 2θ maximums at 4.2°, 4.5°, and 4.9° (Figure 6) appeared after being crystallized for 65−80 min. These were also attributed to the CrII phase.[1] The intensities of all these CrII reflections increased with t_c and remained constant after

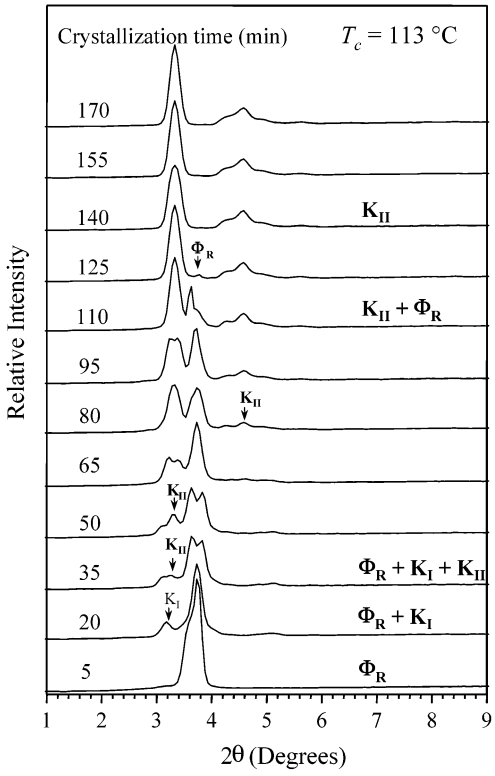

Figure 6. Set of WAXD powder patterns for HOBT-C8 isothermally crystallized at T_c = 113 °C at different t_c values.

reaching 140 min. At the same time, the overlapped (110) and (200) diffractions at 2θ = 3.6° and 3.7°

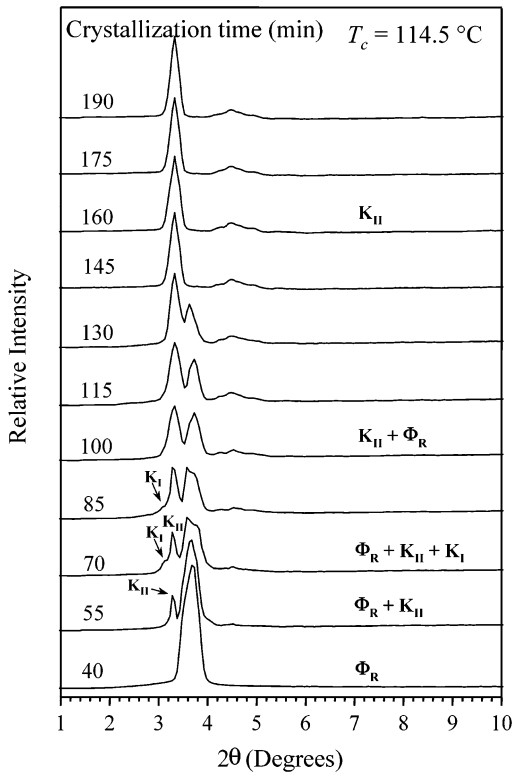

Figure 7. Set of WAXD powder patterns of HOBT-C8 after isothermally crystallized at $T_c = 114.5$ °C at different t_c values.

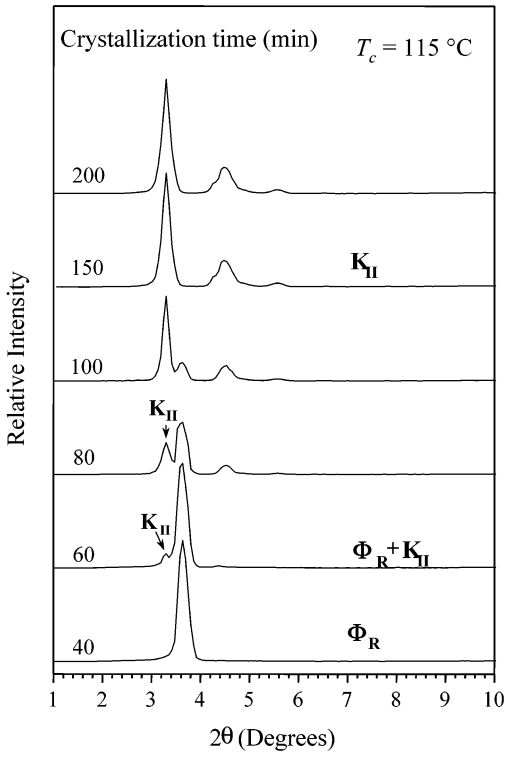

Figure 8. Set of WAXD powder patterns for HOBT-C8 isothermally crystallized at $T_c = 115$ °C at different t_c values.

ascribed to the ColR phases intensities continuously decreased with increasing t_c until they completely disappeared at $t_c = 140$ min (Figure 6). On the other hand, the intensity of the (111) diffraction at $2\theta = 3.2°$ for the CrI phase appeared to increase initially, indicating a growth of the CrI phase. However, after $t_c = 95$ min, this diffraction disappeared revealing the completion of the phase transformation of the CrI → CrII phase. Therefore, Figure 6 provides structural evidence during isothermal crystallization at 113 °C for both phase transformations of the ColR → CrI and the CrI → CrII phases (without heating).

Figure 7 shows the corresponding isothermal 1D WAXD experiments in the low-2θ angle region at $T_c = 114.5$ °C. Before $t_c = 40$ min, only two overlapping (110) and (200) diffractions at $2\theta = 3.6°$ and 3.7° were observed that were again attributed to the ColR phase. After an additional 15-min crystallization period, the sharp (200) diffraction of the CrII phase at $2\theta = 3.3°$ appeared. At $t_c = 70$ min, a shoulder at $2\theta = 3.2°$, which is the characteristic (111) diffraction of the CrI phase, also appeared. With a further increase in t_c, the intensity of this shoulder decreased and disappeared completely after $t_c = 100$ min due to the CrI → CrII phase transformation. Therefore, we arrived at the same conclusion that we obtained from the DSC results at $T_c = 114.5$ °C (compared with the DSC results in Figure 4). Moreover, the intensity of the (200) diffraction at $2\theta = 3.3°$ increased continuously with a corresponding gradual decrease of the intensities and eventual disappearance of the (110) and (200) diffractions at $2\theta = 3.6°$ and 3.7° that were attributed to the ColR phase.

Figure 8 illustrates another set of 1D WAXD patterns during isothermal crystallization at 115 °C. The (111) diffraction at $2\theta = 3.2°$ corresponding to the CrI phase was not observed. The (200) diffraction at $2\theta = 3.3°$ of the CrII phase appeared at $t_c = 60$ min, and its intensity continuously increased with increasing t_c until a maximum was reached after 150 min. The overlapping (110) and (200) diffractions at $2\theta = 3.6°$ and 3.7° of the ColR phase intensities gradually decreased and disappeared after $t_c = 150$ min. This set of WAXD patterns reveals that an exclusive crystallization of the CrII phase at $T_c \geq 115$ °C occurred directly from the ColR phase, and no CrI phase was formed in the entire t_c period.

Overall Phase Transformation Rates. We recognize that we are dealing with three-phase transformations: the ColR → CrI, the CrI → CrII, and the ColR → CrII phases at different T_c values based on the DSC and WAXD results. If we define a logarithmic reciprocal time at which 50% of the crystallinity had developed during the isothermal crystallization as representing the overall rate for each phase transformation, a plot of the $\log(1/t_{50\%})$ vs T_c can be constructed and is shown in Figure 9. Note that the overall rates include both the primary nucleation and crystal growth rates. To calculate the crystallinity, the maxima of the heats of transitions of the ColR → CrI and the ColR → CrII phases needed to be known. They were obtained by extrapolating the heats of transitions to zero of the reciprocal logarithmic t_c ($1/\log t_c$),[37] and they were 5.6 and 19.9 kJ/mol, respectively.

The overall crystallization rates of the CrII phase grown from the CrI phase increased slightly starting at $T_c = 84$ °C, and reached a maximum at 104 °C. After this temperature, the rate $[\log(1/t_{50\%})]$ then began to decrease. Above $T_c = 110$ °C, the overall crystallization rate exhibited a drastic reduction. However, when $T_c <$ 104 °C, the overall crystallization rate of the ColR → CrI phase was too fast to be recorded. Only above $T_c =$

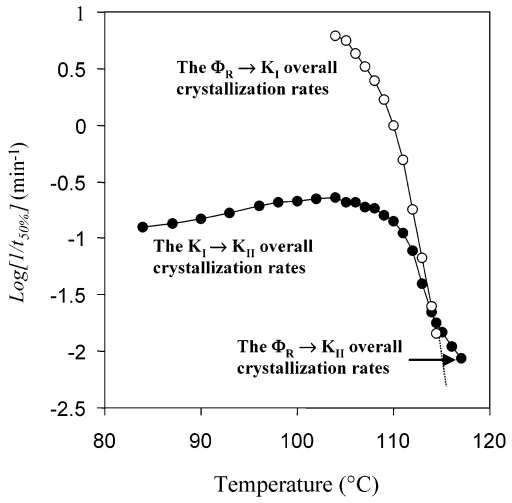

Figure 9. Relationship between the logarithmic reciprocal time in which a 50% crystallinity has developed and T_c for both the CrI and CrII phase formations.

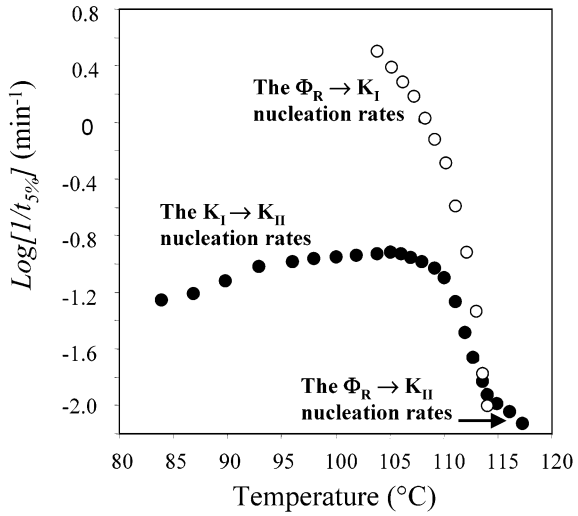

Figure 10. Relationship between the logarithmic reciprocal time in which a 5% crystallinity has developed and T_c for both the CrI and CrII phase formations.

104 °C could the rate be detected, and it was found to monotonically decrease with increasing T_c. When the T_c was above 110 °C, the $\log(1/t_{50\%})$ difference between the formations of the ColR → CrI and the CrI → CrII phases diminished quickly, and, apparently, the formation of these two phases overlapped. In the region of above T_c = 115 °C, the CrII phase formed directly from the ColR phase (see the WAXD results in Figure 8), revealing the overall transformation kinetics of the ColR → CrII phases was faster than that of the ColR → CrI phases. Therefore, the formation of the CrI phase could not be observed (its virtual rate is expressed by the dashed line in Figure 9).

A transition behavior can also be described using a plot between the logarithmic reciprocal t_c at which a 5% of crystallinity had developed, $[\log(1/t_{5\%})]$, and T_c as shown in Figure 10. This value of $\log(1/t_{5\%})$ is commonly referred to as the primary nucleation rate. A similarity of this figure compared with Figure 9 is evident. Therefore, these two figures provide information about interrelationship and interdependence of the ColR → CrI, the CrI → CrII, and the ColR → CrII phase transitions. In the region of low T_c values, the transition between the ColR → CrI and the CrI → CrII transformations occurred sequentially. Namely, the ColR → CrI transformation occurred first, followed by the CrI → CrII transformation. With increasing T_c to between 110 °C ≤ T_c < 114 °C, the ColR → CrI phase transformation rate slowed, and it gradually imposed the limit of the CrI → CrII phase transformation. Therefore, the formation of the CrII phase was determined by how fast the CrI phase was formed from the ColR phase. As a result, the formation rates of the CrII phase observed in Figures 9 and 10 exhibited a drastic decrease. Only after T_c was increased to 115 °C did the CrI phase formation from the ColR phase became extremely slow due to the increased its nucleation barrier. This was mainly because the T_m of the CrI phase is at 121 °C, while the T_m of the CrII phase is at 151 °C. Therefore, the ColR → CrII transformation was experimentally accessible.

Linear Crystal Growth Rates of the CrII Phase. To understand how the molecules made a "choice" between the CrI and CrII phases when they crystallized, observations of crystal growth rates of individual crystalline phases with respect to T_c in PLM were needed. The necessary requirement was that each phase had to possess different textures in PLM to be individually recognized. As reported previously, for the discotic LC HOBT-C8 schlieren, fan-typed, mosaic-like, and low-birefringence spherulite-like textures were observed for the ND, ColR, CrI, and CrII phases, respectively.[1] Some of these PLM morphologies are shown in Figure 11a–c. In particular, Figure 11c shows a snapshot of the CrII crystal growth from the ColR phase at 120 °C for t_c = 200 min. The top part of the figure represents the CrII spherulite-like texture with a low birefringence. Furthermore, it should be noted that the crystal growth rates had to be along specific crystallographic axes and different growth axes may possess different growth rates. In the case of spherulitic growth, it is generally accepted that the radial direction of spherulites represents the fastest growth rate. On the basis of the transmission electron microscopy and electron diffraction results, it can be deduced that in CrII phase, the fastest grow rate was along the *c*-axis.[1]

Figure 12 shows the CrII phase crystal growth rate change with T_c. At low T_c values, the rate gradually increased and reached a maximum of 0.31 μm/s at 107 °C. Above 107 °C, the growth rates decreased and reached a minimum at 114.5 °C. Upon further increasing T_c, the CrII growth rates increased again, and reached a second maximum at 116 °C. Measurements of the crystal growth rates of the CrI phase were very difficult because its growth rates were extremely fast at low T_c values, while at high T_c values its birefringence and texture were similar to those of the ColR phase. However, we qualitatively estimated the ColR → CrI phase growth rates, which are represented by a dashed line in Figure 12. The rate minimum appeared in a narrow temperature region in the vicinity of 114.5 °C where the phase transformation rates of the ColR → CrI phases and the CrI → CrII phases were almost identical. This observation reveals that in this narrow T_c region, the nucleation barriers of both phase transformations were almost equal. Therefore, two choices were given

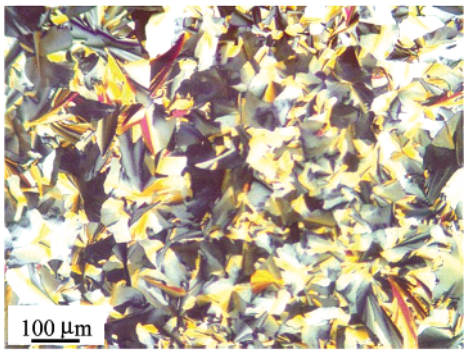

(a) The Φ_R phase at 120 °C

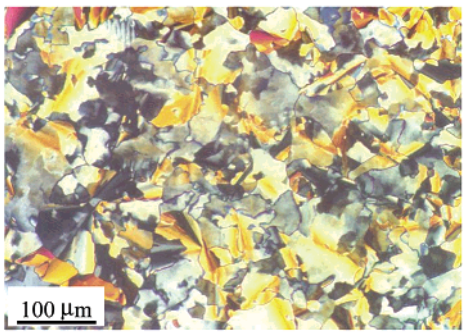

(b) the K_I phase at 100 °C

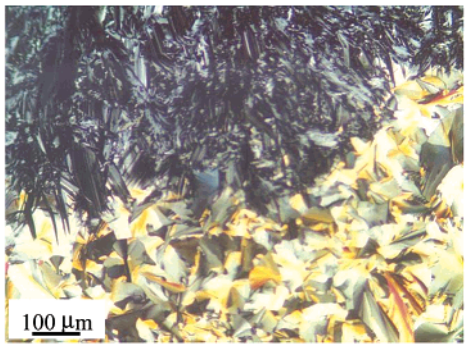

(c) The K_{II} phase grown in the Φ_R phase 120 °C

Figure 11. Sets of PLM morphological textures in different phase structures: (a) in the ColR phase at 120 °C; (b) in the CrI phase at 100 °C; and (c) a snap shot of the CrII phase growth from in the ColR phase at 120 °C and t_c = 200 min. The top half of the figure is a CrII spherulite with a low birefringence.

to each HOBT-C8 molecule during the phase transformation process, and the criterion for the selection was the nucleation barrier height.[38−40] As a result, molecules could either crystallize to form the CrII phase directly from the ColR phase, or they formed the metastable CrI phase first and then transformed into the CrII phase. If two phase transformation processes occur on a growth front of the same crystal, The CrI phase formation *hampers* the growth of the CrII phase (so-called a "self-poisoning effect"). Therefore, the CrII growth rate exhibited a minimum in the vicinity of 114.5 °C due to the competition between the formations of the CrI and CrII structures.

In the past, similar phenomena were observed in the case of a series of liquid crystalline polymers. It was found that a monotropic low-ordered liquid crystalline

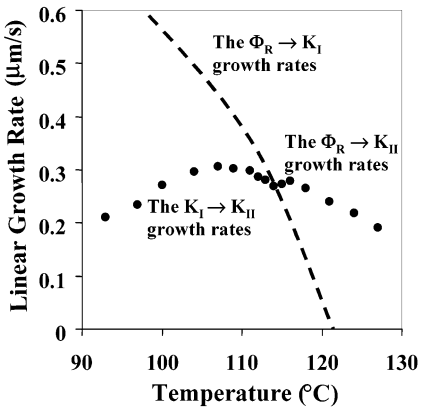

Figure 12. Plot of the growth rate of the CrI → CrII, the ColR → CrII phase transformations versus T_c measured in PLM. The dashed line represents the qualitative transformation rates of the ColR → CrI phases.

phase could substantially enhance the overall crystallization kinetics compared with the crystallization kinetics directly from the I.[39−41] However, in the cases of *n*-alkanes and low-molecular-weight poly(ethylene oxide), linear growth rate minima were found in the vicinity of the transition temperature between the once-folded and the extended chain crystal formations.[42−45] The explanation was that the once-folded chain conformation in the crystal growth front poisoned the growth of the extended chain crystal. In those cases, the crystal structures were identical. This study is the first report of the observation that a monotropic metastable crystal phase, which possessed a different phase structure, could also hamper the linear crystal growth rate of the stable crystal phase to generate a growth rate minimum. Finally, the consistency of the monotropic phase behavior of this system observed in DSC and PLM experiments was surprising to us since in most of the materials studied, different boundaries (such as aluminum surface in DSC and glass surface in PLM experiments) can obscure the phase formation.

Conclusions

In summary, to understand the role of metastability of the transient CrI phase on the transformation kinetics of the CrII phase from the liquid crystalline ColR phase in HOBT-C8, systematic analyses have been carried out using DSC, WAXD, and PLM experimental results. The crystallization of HOBT-C8 was divided into three T_c regions on the basis of their phase transformation rates (including both of the primary nucleation and the overall crystallization rates). In the region III where T_c < 114 °C, the transient, metastable CrI phase always developed prior to the CrII phase despite the fact that the CrII phase is thermodynamically more stable. The molecular packing formations from the ColR phase to the CrII phase via the CrI phase were sequential. Therefore, the ColR → CrI and the CrI → CrII phase transitions were statically coupled. In the region II where 114 °C ≤ T_c < 115 °C, both of the ColR → CrI and the CrI → CrII phase transformation rates were almost identical. More specifically, the nucleation barrier heights of the CrI and CrII phases were almost identical. In this region, the linear crystal growth rates of the CrII phase appeared at a minimum. The CrI

phase formation suppressed the growth of the CrII phase when the two different crystal structures were on a single-crystal growth front. This led to a growth competition between the CrI and CrII phases, and resulted in the rate-minimum caused by "self-poisoning" effect. Therefore, the ColR → CrI and the CrI → CrII phase transitions were dynamically coupled. In region I, where the $T_c \geq 115$ °C, only the CrII phase was formed directly from the ColR phase without passing through the metastable CrI phase. The molecular packing formations again became sequential, but in this case only the ColR and CrII phases were involved.

Acknowledgment. This work was supported by the NSF ALCOM Science and Technology Center (DMR-8920147) at Kent State University, Case Western Reserve University, and University of Akron, NSF (DMR-0203994), and the Nitto Denko Corporation.

References

(1) Tang, B. Y.; Ge, J. J.; Zhang, A.; Chu, P.; Calhoun, B.; Wang, H.; Shen, Z.; Harris, F. W.; Cheng, S. Z. D. *Mater. Chem.* **2001**, *13*, 78.
(2) Chandrasekhar, S.; Sadashiva, B. K.; Suresh, K. A. *Pramana* **1977**, *9*, 471.
(3) Chandrasekhar, S. *Mol. Cryst. Liq. Cryst.* **1981**, *63*, 171.
(4) Destrade, C.; Nguyen Huu Tinh; Gasparoux, H.; Malhtete, J.; Levelut, A. M. *Mol. Cryst. Liq. Cryst.* **1981**, *71*, 111.
(5) Nguyen Huu Tinh; Gasparoux, H.; Destrade, C. *Mol. Cryst. Liq. Cryst.* **1981**, *68*, 101.
(6) Billard, J.; Dubois, J. C.; Vaucher, C.; Levelut, A. M. *Mol. Cryst. Liq. Cryst.* **1981**, *66*, 115.
(7) Pugh, C.; Percec, V. *J. Mater. Chem.* **1991**, *1*, 765.
(8) Giroud-Godquin, A. M.; Billard, J. *Mol. Cryst. Liq. Cryst.* **1981**, *66*, 147.
(9) Piechocky, C.; Simon, J.; Skoulios, A.; Guillon, D.; Weber, P. *J. Am. Chem. Soc.* **1982**, *104*, 5245.
(10) Barbera, J.; Cativiela, C.; Serrano, J. L.; Zurbano. M. M. *Adv. Mater.* **1991**, *3*, 602.
(11) Zhang, H.; Lai, C. K.; Swager, T. *Chem. Mater.* **1995**, *7*, 2067.
(12) Lai, C. K.; Tsai, C.-H.; Pang, Y.-S. *J. Mater. Chem.* **1998**, *8*, 1355.
(13) Ebert, E.; Wendorff, J.; Lattermann, G. *Liq. Cryst.* **1990**, *7*, 553.
(14) Lattermann, G.; Straufer, G.; Brezesinski, G. *Liq. Cryst.* **1991**, *10*, 169.
(15) Ciuchi, F.; Nicola, G. D.; Franz, H.; Gottarelli, G.; Mariani, P.; Bossi, M. G. P.; Spada, G. P. *J. Am. Chem. Soc.* **1994**, *116*, 7064.
(16) Farre-Nicolin, C. D.; Lub, J.; Van der Sluis, P. *Adv. Mater.* **1996**, *8*, 1005.
(17) Destrade, C.; Foucher, P.; Gasparoux, H.; Nguyen Huu Tinh; Levelut, A. M.; Malthete, J. *Mol. Cryst. Liq. Cryst.* **1984**, *106*, 121.
(18) Kreuder, W.; Ringsdorf, H. *Macromol. Chem. Rapid Commun.* **1983**, *4*, 807.
(19) Weck, M.; Mohr, B.; Maughon, B. R.; Grubbs, R. H. *Macromolecules* **1997**, *30*, 6430.
(20) Raja, K. S.; Raghanathan, V. A.; Ramakrishnan, S. *Macromolecules* **1998**, *31*, 3807.
(21) Wang, T.; Yan, D.; Zhou, E.; Karthaus, O.; Ringsdorf, H. *Polymer* **1998**, *39*, 4509.
(22) Disch, S.; Finkelmann, H.; Ringsdorf, H.; Schuhmacher, P. *Macromolecules* **1995**, *28*, 2424.
(23) Ungar, G. *Polymer* **1993**, *34*, 2050.
(24) Zheng, R.; Chen, R.; Cheng, S. Z. D.; Xie, F.; Yan, D.; He, T.; Percec, V.; Chu, P.; Ungar, G. *Macromolecules* **1999**, *32*, 3574.
(25) Zheng, R.; Chen, R.; Cheng, S. Z. D.; Xie, F.; Yan, D.; He, T.; Percec, V.; Chu, P.; Ungar, G. *Macromolecules* **1999**, *32*, 6981.
(26) Zheng, R.; Chen, R.; Cheng, S. Z. D.; Xie, F.; Yan, D.; He, T.; Percec, V.; Chu, P.; Ungar, G. *Macromolecules* **2000**, *33*, 5159.
(27) Carr, N.; Gray, G. W. *Mol. Cryst. Liq. Cryst.* **1985**, *124*, 27.
(28) Andrews, B. M.; Gray, G. W. *Mol. Cryst. Liq. Cryst.* **1985**, *123*, 257.
(29) Ungar, G.; Feijoo, J. L.; Keller, A.; Yord, R.; Percec, V. *Macromolecules* **1990**, *23*, 3411.
(30) Percec, V.; Keller, A. *Macromolecules* **1990**, *23*, 4347.
(31) Cheng, S. Z. D.; Yandrasits, M. A.; Percec, V. *Polymer* **1991**, *32*, 1284.
(32) Yandrasits, M. A.; Cheng, S. Z. D.; Zhang, A.; Cheng, J.; Wunderlich, B.; Percec, V. *Macromolecules* **1992**, *25*, 2112.
(33) Pardey, R.; Zhang, A.; Gabori, P. A.; Harris, F. W.; Cheng, S. Z. D.; Aducci, J.; Facinelli J. V.; Lenz, R. W. *Macromolecules* **1992**, *25*, 5060.
(34) Pardey, R.; Shen, D.; Gabori, P. A.; Harris, F. W.; Cheng, S. Z. D.; Aducci, J.; Facinelli J. V.; Lenz, R. W. *Macromolecules* **1993**, *26*, 3687.
(35) Ge. J. J.; Zhang, A.; McCreight, K. W.; Ho, R.-M.; Wang, S.-Y.; Jin, X.; Harris, F. W.; Cheng, S. Z. D. *Macromolecules* **1997**, *30*, 6498.
(36) Mori, H.; Itoh, Y.; Nishiura, Y.; Nakamura, T.; Shinagawa, Y. *Jpn. J. Appl. Phys.* **1997**, *36*, 143.
(37) Cheng, S. Z. D. *Macromolecules* **1988**, *21*, 2475.
(38) Pardey, R.; Wu, S.; Chen, J.; Harris, F. W.; Cheng, S. Z. D.; Keller, A.; Aducci, J.; Facinelli, J. V.; Lenz, R. W. *Macromolecules* **1994**, *27*, 5794.
(39) Cheng, S. Z. D.; Keller, A. *Annu. Rev. Mater. Sci.* **1998**, *28*, 533.
(40) Keller, A.; Cheng, S. Z. D. *Polymer* **1998**, *39*, 4461.
(41) Jing, A. J.; Taikum, O.; Li, C. Y.; Harris, F. W.; Cheng, S. Z. D. *Polymer* **2002**, *43*, 3431.
(42) Ungar, G.; Keller, A. *Polymer* **1986**, *27*, 1835.
(43) Ungar, G.; Keller, A. *Polymer* **1987**, *28*, 1899.
(44) Organ, S. J.; Ungar, G.; Keller, A. *Macromolecules* **1989**, *22*, 1995.
(45) Cheng, S. Z. D.; Chen, J.-H. *J. Polym. Sci. Polym. Phys. Ed.* **1991**, *29*, 311.

CG020069D